

# China LT1 (LuTan-1) SAR support within GAMMA Software

Urs Wegmüller, Christophe Magnard, Andreas Wiesmann, Gamma Remote Sensing AG

Version 22-Jun-2023 (updated for repeat- and single-pass DInSAR Sections)

## 1. INTRODUCTION

In this document the support provided in the GAMMA Software for the processing of data of the Chinese L-band SAR LT1 (LuTan-1) is summarized. The first LT1 SAR was launched in January 2022, followed by a second one in February 2022.

In Section 2 the importing of the LT1 SLC data is described, followed by an assessment of the data characteristics, in Section 3. In Section 4, the DInSAR processing sequence for a repeat pass interferometric data pair acquired by LT1a and LT1b with a 4-day time interval is presented. In Section 5, a tandem pair consisting of the mono-static reference scene and the corresponding bistatic second scene is interferometrically processed. The main result generated is a terrain height correction relative to a pre-existing DEM.

## 2. IMPORTING LT1 SLC DATA

### 2.1. Importing SLC data

LT1 SLC data are provided as a GeoTIFF with meta data in XML format, that can be read / imported using the program *par\_LTI\_SLC*.

```
par_LTI_SLC LT1A_MONO_KSC_STRIP2_006435_E112.3_N34.5_20230403_SLC_HH_S2A_0000090196.tiff  
LT1A_MONO_KSC_STRIP2_006435_E112.3_N34.5_20230403_SLC_HH_S2A_0000090196.meta.xml  
20230403.slc.par 20230403.slc 0
```

As input, the GeoTIFF and the meta data XML files are indicated. The program generates the SLC binary data file, in SCOMPLEX or FCOMPLEX format, and the related SLC parameter file. The SLC can be visualized using

```
disSLC 20230403.slc 26669 1 - 1. .35 0
```

and the spectrum can be checked using

```
dismph_fft 20230403.slc 26669 1 0 1. .35 128 3 0
```

The orbit state vectors appear to be somewhat "noisy". Possibly, the state vectors correspond to the unfiltered on-board GNSS measurements. To check and improve this, we filter the state vectors using the program *ORB\_filt\_spline.py*. In the present example the number of state vectors is very large, therefore using a spline fit of degree 5 is okay.

```
/bin/cp 20230403.slc.par 20230403.slc.par.orig
```

```
ORB_filt_spline.py 20230403.slc.par.orig 20230403.slc.par --png png_dir --degree 5
```

returns a warning that some outliers were identified. Outliers are state vector values that deviate significantly from the calculated spline fit. The statistics show a meter scale standard deviation of the unfiltered state vector positions from the filtered solution. The generated PNG file with the positional deviations is shown in Figure 1.

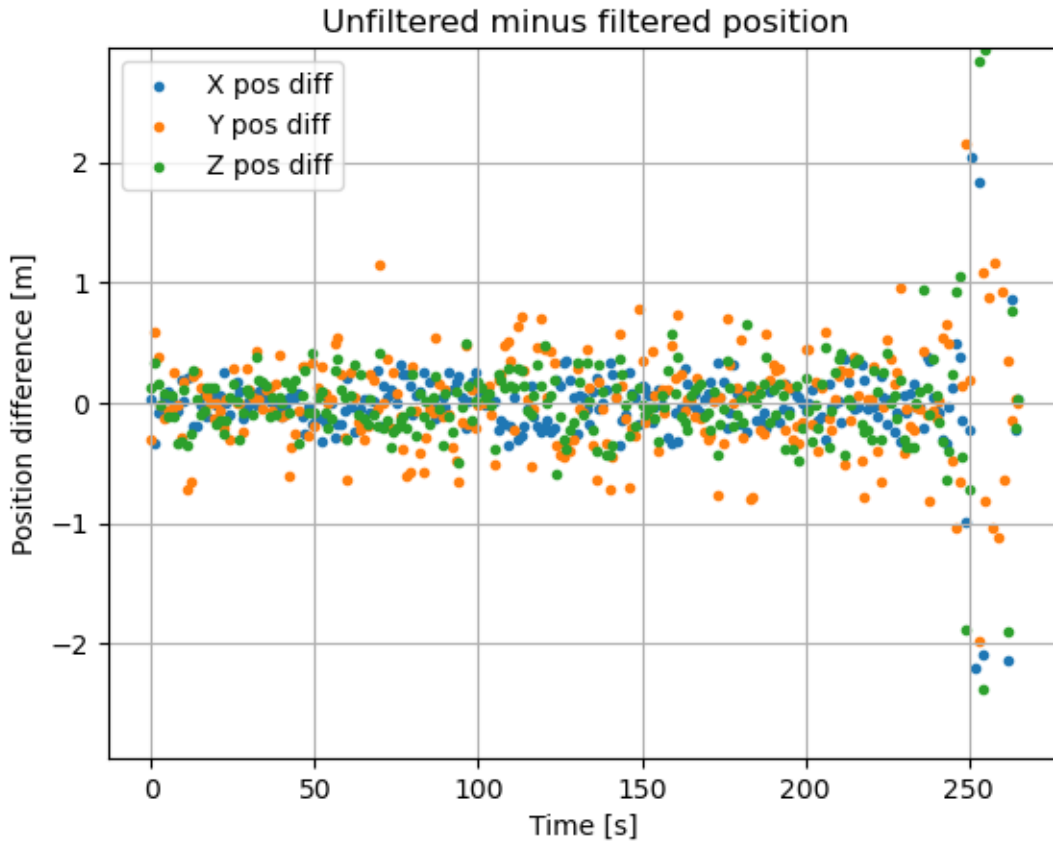


Figure 1 State vector deviations from the filtered solution. There is a noise component of about 0.2m and some outliers with large deviations at the end of the sequence.

We replace the state vectors with filtered state vectors and avoid using the state vectors at the end of the sequence to avoid the outliers:

```
ORB_filt_spline.py 20230403.slc.par.orig 20230403.slc.par --png png_dir --ignore_start 3 --ignore_end 17 --degree 5
```

As a result, we obtain the updated 20211221.slc.par.

Using the SLC we generate a backscatter image in slant range geometry using

```
multi_look 20230403.slc 20230403.slc.par 20230403.mli 20230403.mli.par 5 5 - - 0.00004
ras_dB 20230403.mli 5333 1 5313 1 1 -15. 12 gray.cm 20230403.mli.bmp 0 0
```

A section of the resulting LT1 backscatter image is shown in Figure 2.

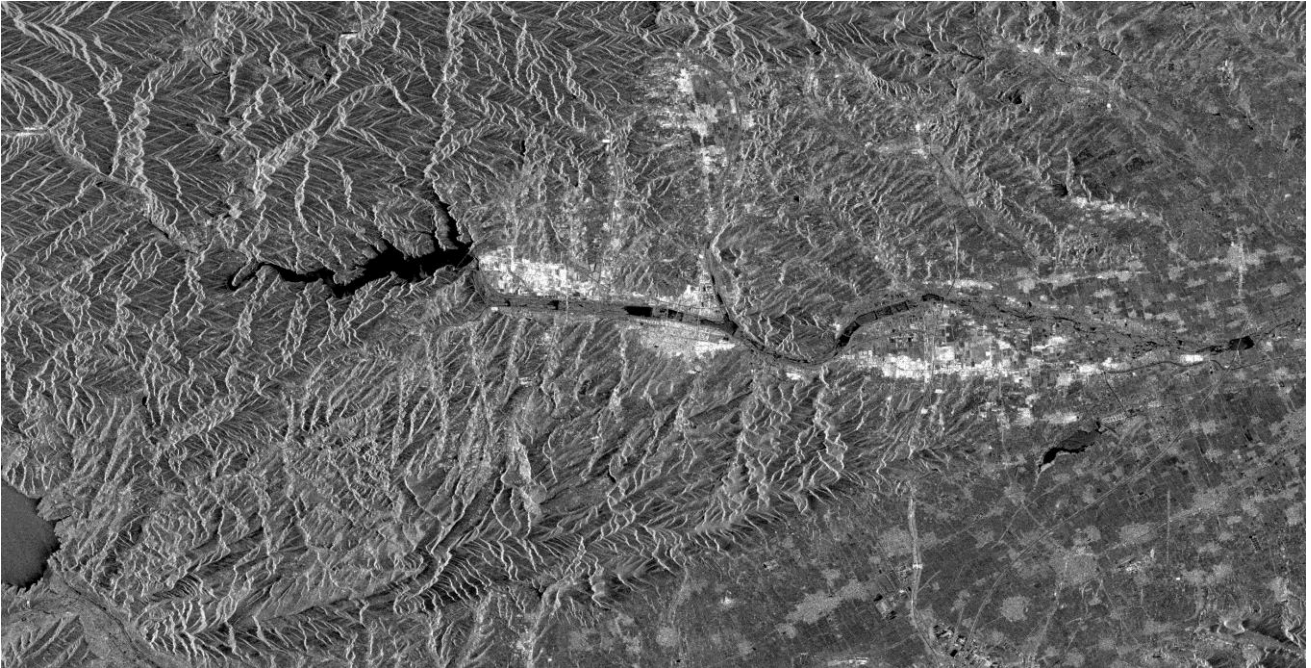


Figure 2 Section of LT1 data (5 x 5 look MLI in slant range geometry).

## **2.2. Importing detected data in slant range geometry**

Not available so far.

## **2.3. Importing geocoded / georeferenced data**

Not available so far.

### **3. ASSESSMENT OF SOME CHARACTERISTICS OF LT1 STRIPMAP SLC**

#### **3.1. Radiometric calibration and estimation of NESZ**

We were (so far) not able to conduct an absolute radiometric calibration for LT1 data. Therefore, the data was not radiometrically calibrated in the SLC reading step. In the *multi\_look* step we conducted a scaling to bring the backscatter to reasonable values. No validation with different satellite data or targets with known backscatter coefficients was done in our assessment.

Using dark areas (radar shadow and smooth water surfaces) we estimated a Noise Equivalent Sigma Zero value. Provided that we did not apply an accurate radiometric calibration there is a certain uncertainty but sufficient to find that the NESZ value is quite low ( $< -20$  dB).

#### **3.2. Point target characteristics**

Considering several small, strong scatterers present in the scene we determined the following point target characteristics:

slant range resolution (3dB):	2.0 m
azimuth resolution (3dB):	3.8 m
peak_side_lobe_ratio:	$< -17$ dB

#### **3.3. Geocoding**

We generated a multi-look intensity image using 5 range and 5 azimuth looks and conducted a geocoding sequence, using the 1-arc-second Copernicus DEM. As part of the geocoding sequence a refinement was determined based on the offset between a simulated backscatter image (calculated based on the orbit data and the DEM) and the actual SAR backscatter.

The refinement statistics indicate for the offset estimates a very small standard deviation of below 0.1 multi-look pixel in both slant range and azimuth directions. For the data acquired in 2023, the determined range and azimuth offsets was also small ( $< 20$ m), while a substantial azimuth offset (350 multi-look pixels) was found for the data acquired in 2022. A geocoded backscatter image is shown in Figure 3 and a small section of it in Figure 4. Because of the mountainous terrain a large fraction of the area is in layover.

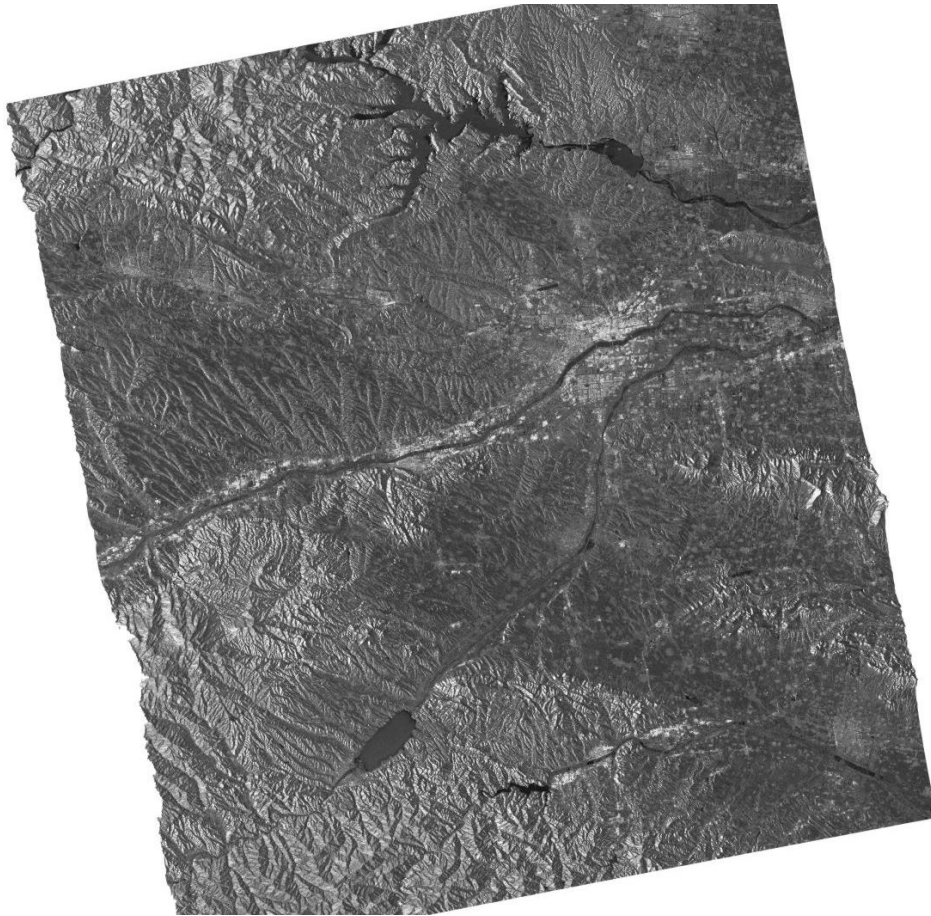


Figure 3 Geocoded LT1 backscatter.



Figure 4 Small section of geocoded LT1 backscatter.

## 4. LT1 REPEAT-PASS DIFFERENTIAL SAR INTERFEROMETRY (DINSAR)

### 4.1. Processing sequence used

We were able to test LT1 differential SAR interferometry using an LT1 pair with 4 days difference and a perpendicular baseline component of about 650m, acquired on 17. and 21. March 2023 over the southern part of Gansu Province, China.

A flow chart of the processing sequence used is shown in Figure 5. In the following, some of the steps are further discussed.

The two scenes used were acquired by LT1A (second scene, 21. March 2023) and LT1B (reference scene, 17. March 2023). The importing of the two SLCs is done using the program *par\_LT1\_SLC*. After the importing we checked and filtered the orbit state vectors. In the case of the LT1A scene, the corrections applied in the filtering were quite substantial (meter scale for a few of the state vectors). In the case of the LT1B scene the corrections were smaller (cm scale) but still significant. Applying the state vector filtering with the program *ORB\_filt\_spline.py* a second time was used to check if the first application was successful, in the sense that corrections of a second application were negligible.

We selected then the earlier scene as the reference, generated a multi-look intensity image (MLI) with 5 range and 5 azimuth looks, and conducted a geocoding sequence using the Copernicus 30m global DEM. This also included the resampling of the DEM height into the MLI geometry.

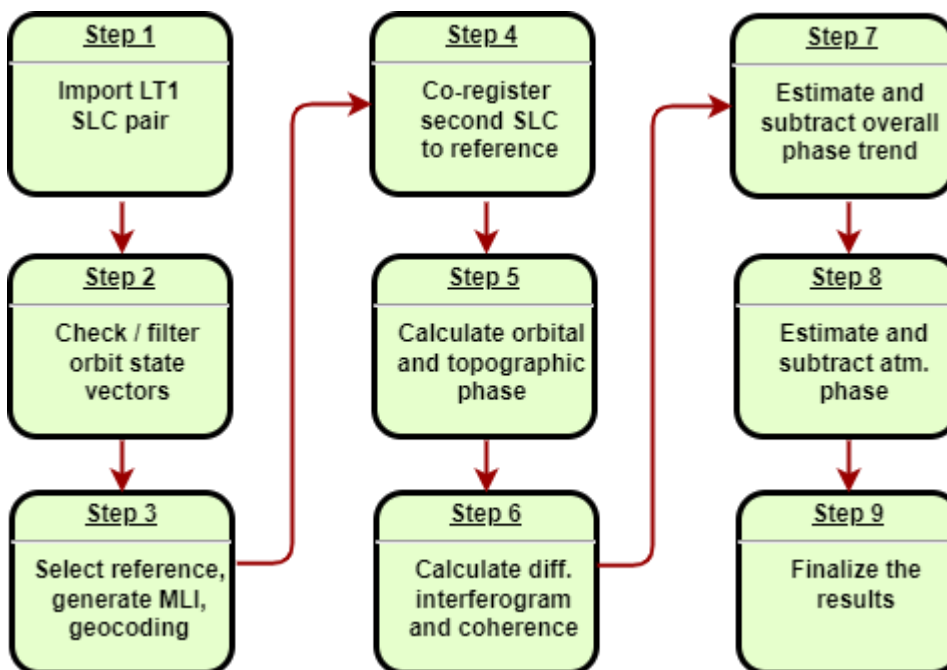
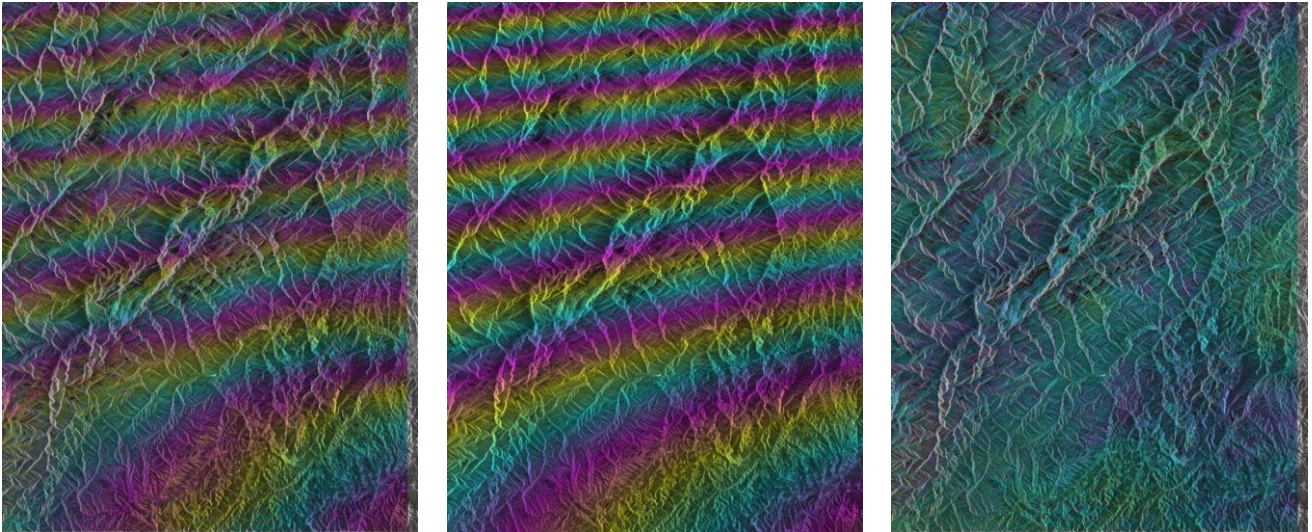


Figure 5 Flowchart of DInSAR processing sequence used.

Next, we co-registered the second SLC to the reference SLC. In this we used a sequence that also considers the terrain height (using *rdc\_trans*). In this a refinement is done using intensity matching, to achieve a co-registration accuracy better than 0.2 SLC pixel.

Then we calculated the orbital and topographic phase (*phase\_sim\_orb*) and the differential interferogram (*SLC\_diff\_intf*). The resulting differential interferogram has a high coherence but shows a quite substantial overall phase trend, mainly in the azimuth direction (Figure 6a). We unwrap the differential interferogram (*mcf*), estimate the overall phase trend (*quad\_fit*, Figure 6b), and subtract it (*sub\_phase*), to get the “detrended” differential interferogram (Figure 6c).

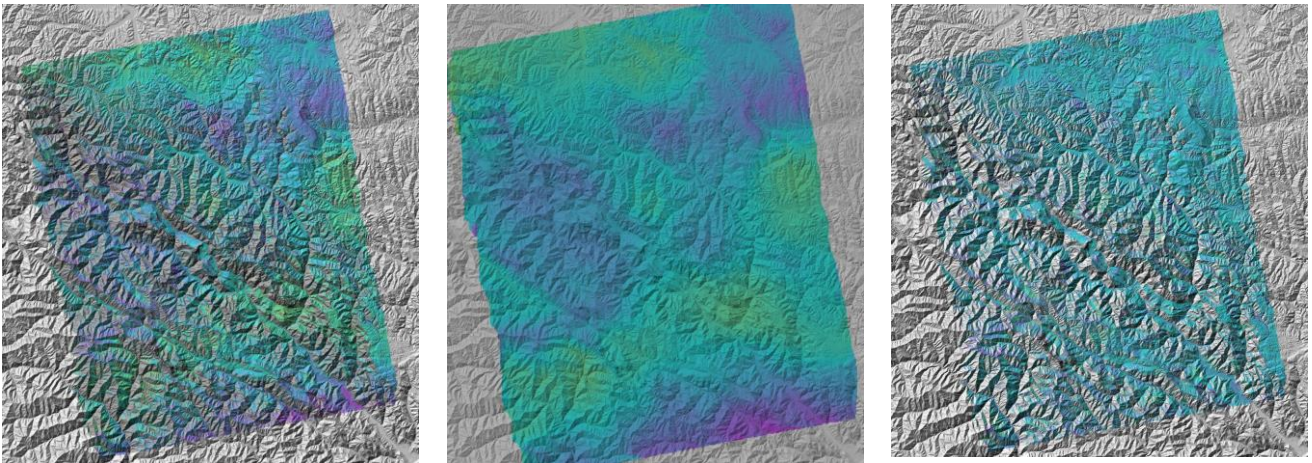


a) differential interferogram

b) estimated trend

c) detrended interferogram

Figure 6 “Detrending” of LT1 differential interferogram.



a) geocoded, detrended differential interferogram

b) estimated atmospheric phase

c) detrended and atmosphere corrected interferogram

Figure 7 In map geometry, the atmospheric phase is estimated and subtracted to get the geocoded, detrended and atmosphere corrected differential interferogram. In addition, layover and shadow areas have been masked.

Starting from the “detrended” differential interferogram we estimate an atmospheric path delay. For this the complex-valued differential interferogram and the coherence map are geocoded and unwrapped. Based on the unwrapped phase, the atmospheric path delay phase is estimated, including

a height dependent and a turbulent (low frequency) term, and subtracted from the “detrended” differential interferogram. Furthermore, the layover and shadow areas are masked to avoid noisy phase in these areas.

### 4.2. Landslide Example

The main interest in the differential interferogram is the identification and quantification of ground-displacements. Now in the present interferometric pair the time interval is short (4 days) and the wavelength long – consequently, the sensitivity to displacements is low. Or in other words the pair is only suited to identify very fast-moving displacements. By visually checking the data, we identified a very clear displacement signal. Figure 8 shows the related small section of the geocoded differential interferogram.

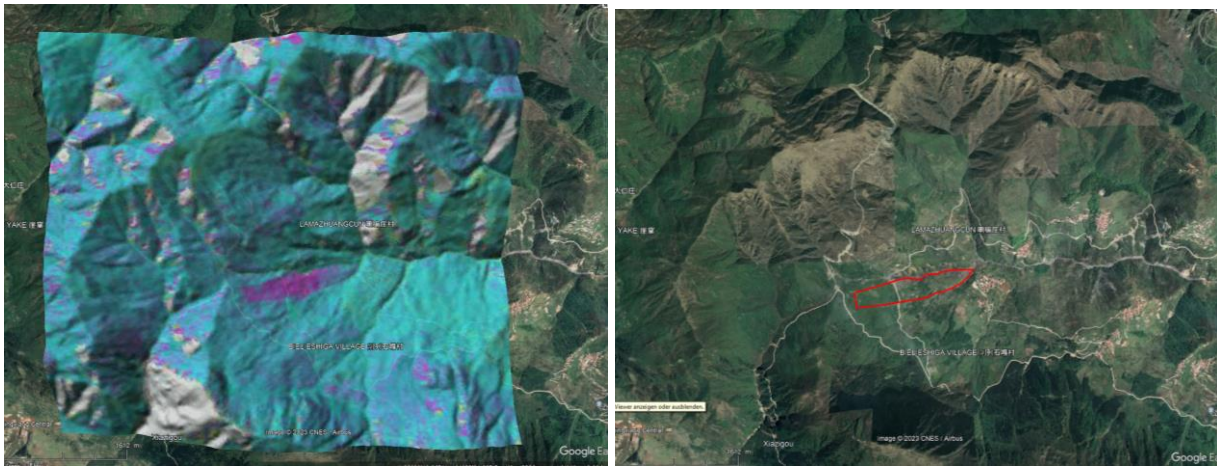


Figure 8 The image to the left shows the geocoded LT1 differential interferogram (dt=4days, Bper=650m, 17.3.2023-21.3.2023), the image to the right a polygon delineating the landslide on top of optical imagery from Google Earth. The line-of-sight velocity of the landslide is > 1 cm per day.

### 4.3. Discussion

The example investigated clearly confirms that LT1 can be used for SAR interferometry, also in a combination of LT1A and LT1B satellites.

Thanks to the short time interval and the relatively short spatial baseline the coherence of the interferogram is high.

The small section shown in 4.2 confirms that the data is suited for displacement mapping. A fast-moving landslide could be identified, mapped and an approximate velocity could be estimated.

This also worked for the forested part of the landslide. Thanks to the L-band frequency and the short temporal and spatial baseline the coherence was high.



## 5. LT1 SINGLE-PASS DIFFERENTIAL SAR INTERFEROMETRY (DINSAR)

### 5.1. Processing sequence used

After the launch of LT1b in 2022 the two L-band SAR sensors LT1a and LT1b were operated in a Tandem mode with one sensor transmitting and receiving (monostatic acquisition) and the other one also receiving the signal transmitted by the first (transmitting) sensor (bistatic acquisition). Combining the monostatic and bistatic acquisitions support single-pass interferometry. Single-pass interferometry with a spatial baseline can be used to determine topographic heights. Examples for this are the SRTM DEM that was generated using the single-pass C-band acquisitions and the Copernicus DEM that is uses X-band single-pass acquisitions acquired by the Tandem-X satellite constellation.

For our testing we had a single pass LT1a/LT1b tandem pair acquired with a perpendicular baseline component of about 2400m, acquired on 14. Oct. 2022 over the Bailong River in southern part of Gansu Province, China.

A flow chart of the processing sequence used is shown in Figure 9. In the following some of the steps are further discussed.

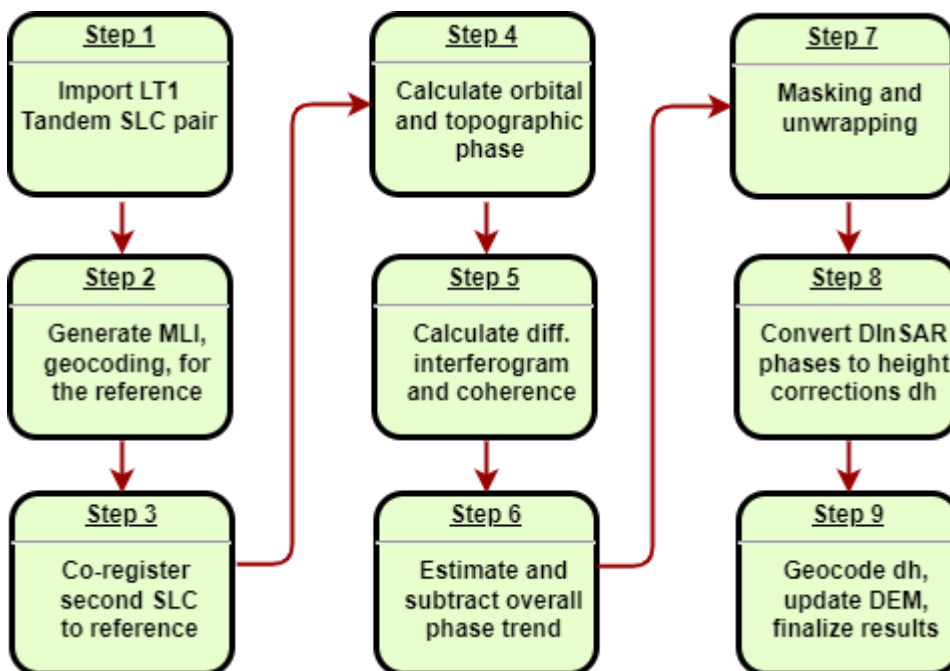


Figure 9 High-level flowchart of DInSAR processing sequence used to update a pre-existing DEM based on a LT1 Tandem pair.

The importing of the scenes is done using the program *par\_LT1\_SLC*. Importing of the bistatic scene is done in the same way as for the monostatic scene. With the bistatic acquisition, XML files with meta data are provided per data set. In addition, a third XML is provided with a name that includes LT1AB. Among other things this file informs about which one of the two sensors is the monostatic

(active) and which one the bistatic (passive) sensor. In our example LT1a is the active sensor, so we use LT1a as the reference of the single-pass interferometric pair.

As for other LT1 SLC data we recommend to check/filter the orbit state vectors immediately after reading the data (to assure that the filtered state vectors are present e.g. in the MLI parameter file). This checking/filtering is done using the program *ORB\_filt\_spline.py*. In our example there was for both scenes for one coordinate a saw tooth deviation with a magnitude of about 5cm. We think that this may be related to a quantization issue (not of the state vectors provided with the data but with a previous intermediary element used in the navigation data processing).

The monostatic scene is selected as the reference, a multi-look intensity image (MLI) with 5 range and 10 azimuth looks is generated, and a geocoding sequence using the Copernicus 30m global DEM is conducted. This also included the resampling of the DEM height into the reference MLI geometry.

In the co-registration of the second scene, which is the bistatic acquisition, to the reference, we have to consider that the second scene is not a different monostatic scene but a bistatic scene. For the bistatic acquisition, the two-way slant range is the sum of the slant ranges from the first orbit to the target ( $r_1$ ) and from the target to the second orbit ( $r_2$ ). So the “effective slant range” is  $(r_1+r_2)/2$  (and not  $r_2$ ). A co-registration procedure using the older version of *rdc\_trans* was implemented in *SLC\_coreg\_tandem.py*. Starting with the Dec. 2023 release, updated versions of *rdc\_trans* and *SLC\_coreg.py* with a “tandem mode option” will be available in the software.

In the co-registration of a pair with a long spatial baseline, considering the terrain topography effects is relevant. Using a constant height instead of a DEM or using a DEM with significant errors may result in imperfect co-registration. Co-registration errors  $> 0.2$  pixel in slant range result in a reduction of the coherence, errors  $> 1$  pixel may result in a complete decorrelation. Doing the processing without a DEM, assuming a constant height, seems reasonable. A refinement step would then be applied based on an offset field estimated using *offset\_pwr\_tracking*.

After the co-registration, the simulation of the orbital and topographic phase is done using *phase\_sim\_orb*. Here it is important that the “single-pass mode” is used. Using the co-registered SLC and the simulated orbital and topographic phase we can then calculate the single-pass differential interferogram (using *SLC\_diff\_intf*). For a single-pass interferogram there is no temporal decorrelation, so we expect that the coherence is very high. Low coherence is observed for layover and shadow areas, for areas with very low backscatter (e.g. smooth water surfaces and wet snow). Non-overlapping parts of the reflectivity spectra may also reduce the coherence (depending on the perpendicular baseline component) and for areas with significant volume scattering the coherence may also be reduced (by “volume decorrelation”), again depending on the length of the perpendicular baseline component.

It may be necessary to correct the single-pass differential interferogram for a slight overall phase trend (possibly related to atmospheric effects, orbit errors, processing effects).

After getting the single-pass differential interferogram phase, it needs to be unwrapped. In layover/shadow areas, and very close to such areas the phase is very noisy. It is recommended to mask layover and shadow areas and as well areas with low coherence. A section of the single-pass differential interferogram before and after the masking is shown in Figure 10. The resulting area can be unwrapped using *mcf*, or if phases are all in the interval  $(-\pi, \pi)$  using *cpx\_to\_real*. The phase values can then be converted to height corrections using *dh\_map\_orb*. With a perpendicular baseline of 2400 m the phase to height sensitivity of the single-pass DInSAR phase is about 0.18 radian/meter.

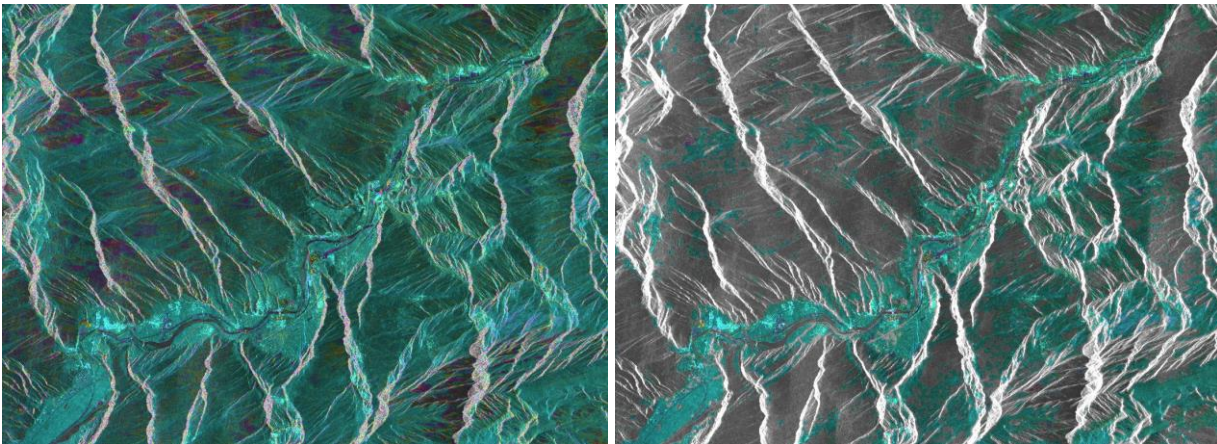


Figure 10 The images show a section of an unmasked (left) and masked (right, layover/shadow and coherence < 0.5 are masked) single-pass LT1 differential interferogram (Bperp=2400m, 14-Oct-2022).

Now the height corrections need to be geocoded from the slant-range MLI geometry to the map geometry. Using the lookup table calculated in the normal geocoding sequence (using the available external DEM, i.e. uncorrected heights) is not precise. The new, corrected DEM heights now available in the slant-range MLI geometry should be used. This is possible using *gc\_inсар*. The calculated lookup table is in the dimension of the slant-range MLI image and the values correspond to the corresponding locations in the map geometry. A refinement of the lookup table can be done by resampling the MLI to the map geometry and determining offset parameters using a matching procedure of the transformed MLI and the previously geocoded backscatter using the DEM. The specific commands used in the related demo example are:

```
lin_comb 2 LT1A_20221014.hgt LT1A_20221014_LT1B_20221014.dh 0. 1. 1. LT1A_20221014.hgt1 3280 1 - 1 1 1
gc_inсар LT1A_20221014.slс.par LT1A_20221014_LT1B_20221014.off LT1A_20221014.hgt1 BailongRiver.dem_par
LT1A_20221014.lt
geocode LT1A_20221014.lt LT1A_20221014.mli 3280 BailongRiver.mli.sim 5016 4955 2 0
create_diff_par BailongRiver.dem_par BailongRiver.dem_par refinement.diff_par 2 0
offset_pwrn BailongRiver.mli.sim BailongRiver.LT1A_20221014.mli refinement.diff_par offs ccp 128 128 - 2 64 64
offset_fitm offs ccp refinement.diff_par - - 0.2 3 0
gc_map_fine LT1A_20221014.lt 3280 gc_inсар_refinement.diff_par LT1A_20221014.lt_fine 1
```

and then the height corrections can be resampled into the map geometry using

```
geocode LT1A_20221014.lt_fine LT1A_20221014_LT1B_20221014.dh 3280 BailongRiver.dh 5016 4955 0 0
```

In the map geometry, the corrections can then be added to the pre-existing DEM heights. The updated DEM is shown in Figure 11 and compared to the Copernicus DEM in Figure 12. The difference to the Copernicus is quite small – in some areas the higher spatial resolution of the update is visible, furthermore small local corrections are visible.

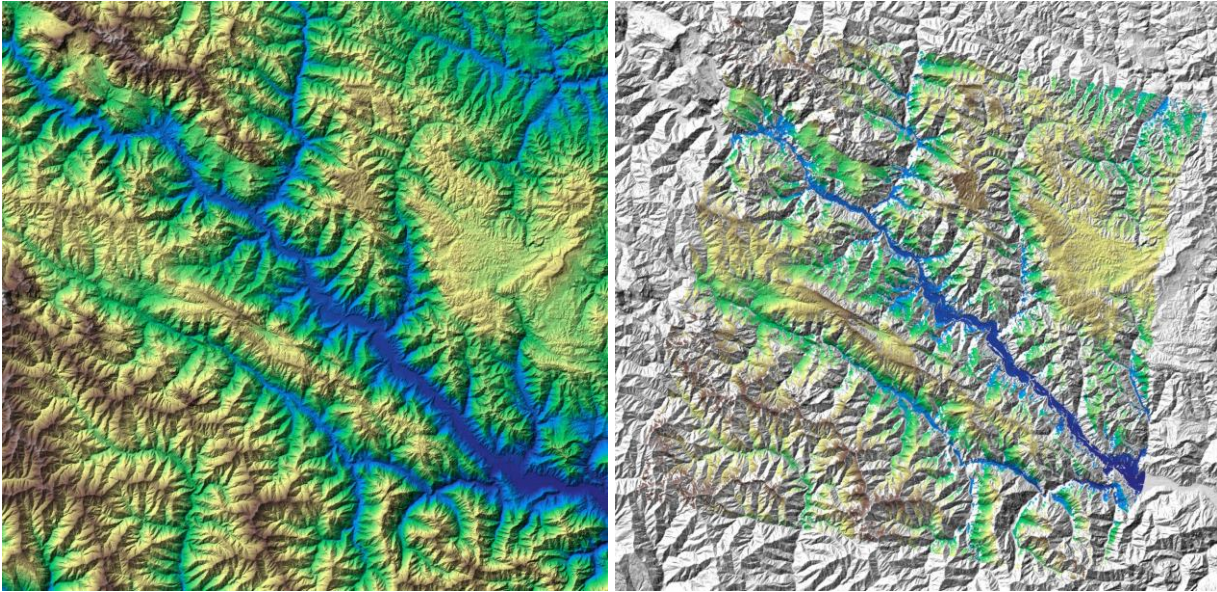


Figure 11 The image to the left shows the updated DEM (sampled at about 15m) which is a combination of the pre-existing DEM (30m Copernicus DEM) and the LT1 Tandem data-based update. The image to the right shows the same, but with color only for areas where the height was updated (and gray scale for areas without update).

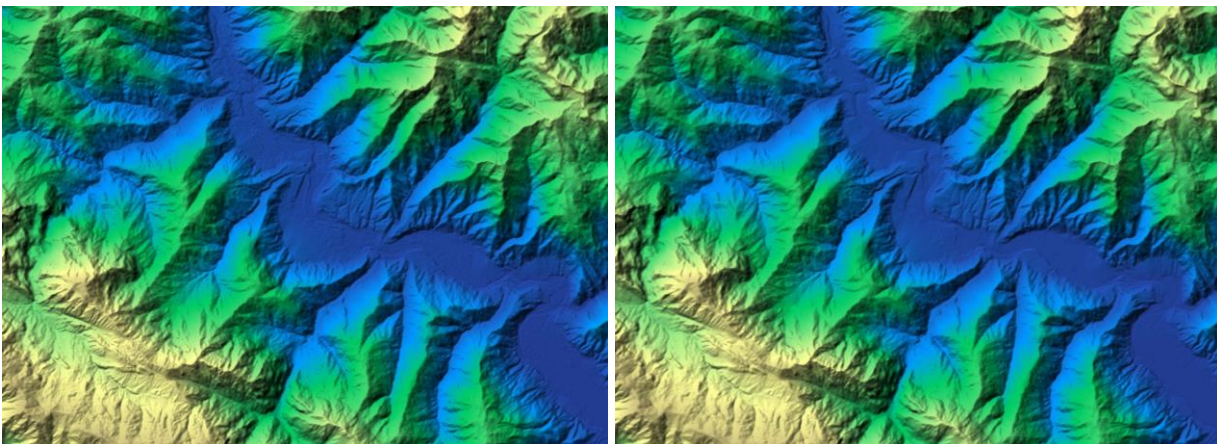


Figure 12 The image to the left shows the updated DEM the image to the right the pre-existing DEM (Copernicus DEM). The section shown is about 16 km x 12 km.

## 6.2 Discussion

The single-pass example investigated clearly confirms the successful operation of the LT1a and LT1b as a constellation. The bistatic scene, the related meta data, and the resulting L-band Tandem interferogram are of good quality. The processing sequence confirms that updating of a pre-existing DEM can be achieved.

To achieve a high quality DEMs over an area in a robust manner, it would be necessary to use multiple Tandem pairs including both ascending and descending orbit. With a single orbital direction, the spatial coverage in mountainous areas is limited by layover and shadow effects.

## **6. ACKNOWLEDGMENT AND COPYRIGHTS**

Professor Daqing Ge's team at China Aero Geophysical Survey and Remote Sensing Center for Natural Resources, is acknowledged for providing access to the LT1 data used.